The Astronomical Journal, 145:167 (15pp), 2013 June doi:10.1088/0004-6256/145/6/167

SIGNS OF ACCRETION IN THE ABUNDANCE PATTERNS OF THE COMPONENTS OF THE RS CVn-TYPE ECLIPSING BINARY STAR LX PERSEI

Young-Woon Kang[1], Alexander V. Yushchenko[1], Kyeongsoo Hong[1,2], Edward F. Guinan[3], and Vira F. Gopka[4]
[1] Department of Astronomy, Sejong University, Seoul 143-747, Korea; kangyw@sejong.ac.kr, yua@sejong.ac.kr
[2] Korea Astronomy and Space Science Institute, Daejeon 303-348, Korea
[3] Department of Astronomy & Astrophysics, Villanova University, Villanova, PA 19085, USA
[4] Astronomical Observatory, Odessa National University, Odessa 65014, Ukraine
Received 2012 October 11; accepted 2013 February 9; published 2013 May 16

ABSTRACT

We present spectroscopic observations of LX Per carried out using the Korean Bohyunsan Observatory Echelle Spectrograph (BOES) with spectral resolving power $R = 80{,}000$. The spectrograph was attached to the 1.8 m telescope. The fit of synthetic spectra to the observed spectrum of the system allowed us to find the component parameters and the abundances of chemical elements in the atmospheres of the components. The strong Ca II H&K emissions are confirmed; we also found emission lines in the Ca II reversals' triplet absorptions at the wavelengths of 8498, 8542, and 8662 Å in the spectrum of the cooler component of LX Per. A unique photometric solution using the distorted light curves of three different epochs was made. The spot model light curves were fitted to the 1981, 1982, and 1983 observations successfully by adjusting only spot parameters. We could infer that the variation of spot location and size was the main reason for the changing shape of light curves. The main feature of the abundance patterns of both components was the apparent deficiency of heavy ($Z > 30$) elements. Only elements with strong lines, namely Y and Ba, were detected. Correlations of relative abundances of chemical elements with condensation temperatures and second ionization potentials of these elements, which can be explained by the accretion of dust and gas, were found.

Key words: accretion, accretion disks – binaries: general – stars: abundances – stars: chemically peculiar – stars: chromospheres – starspots

Online-only material: machine-readable and VO tables

1. INTRODUCTION

LX Persei is a bright eclipsing binary with G0V- and K0IV-type components (Weiler 1974). Its *Hipparcos* parallax, proper motions (Perryman et al. 1997), and radial velocity allow us to estimate its space velocities with respect to the Galactic center as $U = -35 \pm 3$ km s^{-1}, $V = 210 \pm 5$ km s^{-1}, and $W = -15 \pm 2$ km s^{-1}. These velocities and the position of LX Per in the Galaxy clearly state that the system belongs to the Population I stars.

The chemical composition of Population I main-sequence stars resembles the solar abundance patterns of stars with mainly convective energy transport in their outer layers and shows a variety of chemical anomalies for the stars where radiative transport is dominant, namely, for stars with temperatures higher than approximately 6500–8000 K. Even this wide temperature interval is not limited by strict values. For example, Procyon, with an effective temperature of 6591 ± 43 K shows convective motions (Chiavassa et al. 2012), but the coolest Ap star, Przybylski's star, despite a lower value of effective temperature $T_{\rm eff} = 6400$ K (Shulyak et al. 2010), exhibits a variety of anomalies that are usually observed in hotter stars where radiative energy transport clearly dominates.

The hotter component of LX Per is not as peculiar as Przybylski's star is, which is why we can accept that convection is the main phenomenon that should be taken into account to explain the structure of its outer zone.

The origin of chemical abundance anomalies in main-sequence stars with mainly radiative outer layers can be described by diffusion theory (Michaud 1970, 2004), but accretion is also discussed as an additional physical phenomenon, which can explain the variety of abundance patterns for these objects. Various types of accretion were discussed. As an example, it is possible to mention the accretion of interstellar gas (Greenstein 1949; Böhm-Vitense 2006); mass transfer from a binary companion (Fowler et al. 1965; Proffitt & Michaud 1989); the accretion of rocky material, asteroids, and planets (Drobyshevski 1975; Cowley 1977); the dust–gas separation mechanism (Venn & Lambert 1990, 2008); the accretion of accelerated particles (Goriely 2007); etc.

Usually, it is difficult to select the proper accretion scenario, which is why knowledge of the evolutionary status of the investigated object and the conditions in the surrounding interstellar environment is very important. Investigations of binary stars can provide detailed information for constraining the accretion model.

Eclipsing binaries give us information about their stellar parameters, including masses, radii, and luminosities, as well as their distances. We can deduce an accurate relative radius of each component star using the light curves obtained from photometry, while the radial velocity curves obtained from double line spectroscopic observations give us mass ratios and semi-major axes in kilometers. The absolute radii of stars can then be found from their fractional radii ($r = R/A$) since the semi-major orbital axis (A) is known.

Therefore, we can find the absolute dimensions and the distances of binary systems by combining both photometric and spectroscopic results (Kang 2008, 2010). Distances determined from eclipsing binaries are not problematic in terms of the zero point. However, many distances determined from eclipsing binaries still have calibration problems in that the temperature of the primary star is deduced from the spectral type of the

Table 1
Iron Lines in the Spectrum of LX Per

λ (Å)	log gf	Ref.	E_{low} (eV)	Eq. W. (mÅ) Hot	Eq. W. (mÅ) Cool	log $N_{\log N(H)=12}$ Hot	log $N_{\log N(H)=12}$ Cool
			Fe I lines				
4946.385	−1.170	r1	3.368		100		7.558
4969.916	−0.710	r1	4.217		70		7.294
5044.211	−2.017	r2	2.851		74		7.206
5090.773	−0.440	r2	4.256		88		7.496
5242.491	−0.967	r2	3.634		90.5		7.345
5307.361	−2.987	r2	1.608	41		7.509	
5373.709	−0.840	r2	4.473		67.5		7.544
	...	...	...				

(This table is available in its entirety in machine-readable and Virtual Observatory (VO) forms in the online journal. A portion is shown here for guidance regarding its form and content.)

binary system and spectral-type (or color)–$T_{\rm eff}$ calibrations have to be used.

In this paper, we investigate the detached eclipsing binary system LX Per (HIP 15003), which is a double line spectroscopic and eclipsing binary with an orbital period of about 8 days.

The eclipse nature of LX Per was discovered by Ströhmeier (1962). The B and V photoelectric observations were carried out by Ibanoglu et al. (1983) in 1981 and 1982. Túmer et al. (1985) secured the B and V light curves in 1985 and reported a wave-like distortion during the outside eclipse portions of their light curves. Other photometric observations have been published by Percy & Welch (1982), Percy (1985), Poe & Eaton (1985), Caton (1986), and Popper (1988).

Weiler (1974) found double line radial velocity curves in the system using 10 obtained spectrograms and found the mass ratio of the system of $m_{\rm cool}/m_{\rm hot} = 1.04 \pm 0.04$. Later, Weiler (1978) reported variable Ca II H&K emission lines. Popper (1988) completed the double line radial velocity curves using two series of spectrograms obtained from 1966–1972 and 1982–1986 and presented absolute dimensions and a mass ratio of 1.07 ($m_{\rm cool}/m_{\rm hot}$).

The paper is structured as follows:

First, using the new high-resolution spectrum of LX Per, effective temperatures; surface gravities; and microturbulent, rotational, and radial velocities of the components were found. Our spectrum clearly demonstrates calcium emission lines in this RS CVn-type system.

Second, the new solution of published brightness and radial velocity observations of the system allowed us to construct a unique photometric solution for several epochs when the light curves presented a different morphology.

Third, the chemical composition of both components was found using a spectrum synthesis method. The abundance patterns allowed us to conclude that the accretion of dust and gas on the outer layers of components was clearly observed in this system.

2. SPECTROSCOPIC OBSERVATIONS

Spectroscopic observations were carried out with the Bohyunsan Observatory Echelle Spectrograph (BOES) attached to the 1.8 m telescope at the Bohyunsan Observatory of the Korea Astronomy and Space Science Institute (KASI). The spectrograph and observational technique were described by Kim et al. (2000). Basically, the instrument is a moderate-beam, fiber-fed high-resolution spectrograph that incorporates three STU Polymicro fibers of 300, 200, and 80 μm core diameters. These fibers provide spectral resolutions of about $R = \lambda/\Delta\lambda = 30{,}000$, 45,000, and 90,000, respectively. The full working wavelength range of the instrument is from 3500 Å to 10000 Å.

One spectrum of LX Per was obtained at JD 2453368.9545 (mid-exposure) with an exposure time of 50 minutes. It was permitted to reach a signal-to-noise ratio (S/N) of 100–110 at wavelengths 5500–6000 Å, an S/N of 50 at 4150–9500 Å, and an S/N of 20 at 3800 Å. The wavelength range of the spectrum is 3800–9500 Å. Spectral resolving power at the moment of observation was estimated using the telluric lines of Earth atmosphere, and it appeared to be near $R = 80{,}000$.

The primary reduction of the CCD images containing echelle spectra of the program star was carried out using the image processing system IRAF (Tody 1986). The procedure of continuum placement was described by Kang et al. (2012). An example of the spectrum is shown in Figure 1.

3. PARAMETERS FROM HIGH-RESOLUTION SPECTRA

We calculated the synthetic spectra for both component stars of LX Per over the entire observed wavelength region and co-added it to compare with the observed spectrum. To find more reliable information from our observations, we iterated the calculation of synthetic spectra until the best fit to the observed spectrum was achieved. The values of $T_{\rm eff}$ and log g given by Popper (1988) were employed as initial (starting) values. We used detailed descriptions of spectral line lists, and the programs employed can be found in our previous papers, for example, in Yushchenko et al. (1999, 2004), Gopka et al. (2004), and Kang et al. (2012).

3.1. Temperatures, Gravities, Iron Abundances, and Microturbulences

Calculations of iron abundances obtained with different atmosphere models were used to find more precise values of the component parameters ($T_{\rm eff}$, log g, [Fe/H], $\upsilon_{\rm micro}$). The list of iron lines used for this procedure can be found in Table 1. The columns are wavelength, oscillator strength and reference, excitation energy, observed equivalent widths, and calculated iron abundances for two components. The chemical abundances were calculated using the final values of the atmospheric parameters. The table contains 61 and 72 lines of Fe I and eight and six lines of Fe II for hotter (A) and cooler (B) components, respectively.

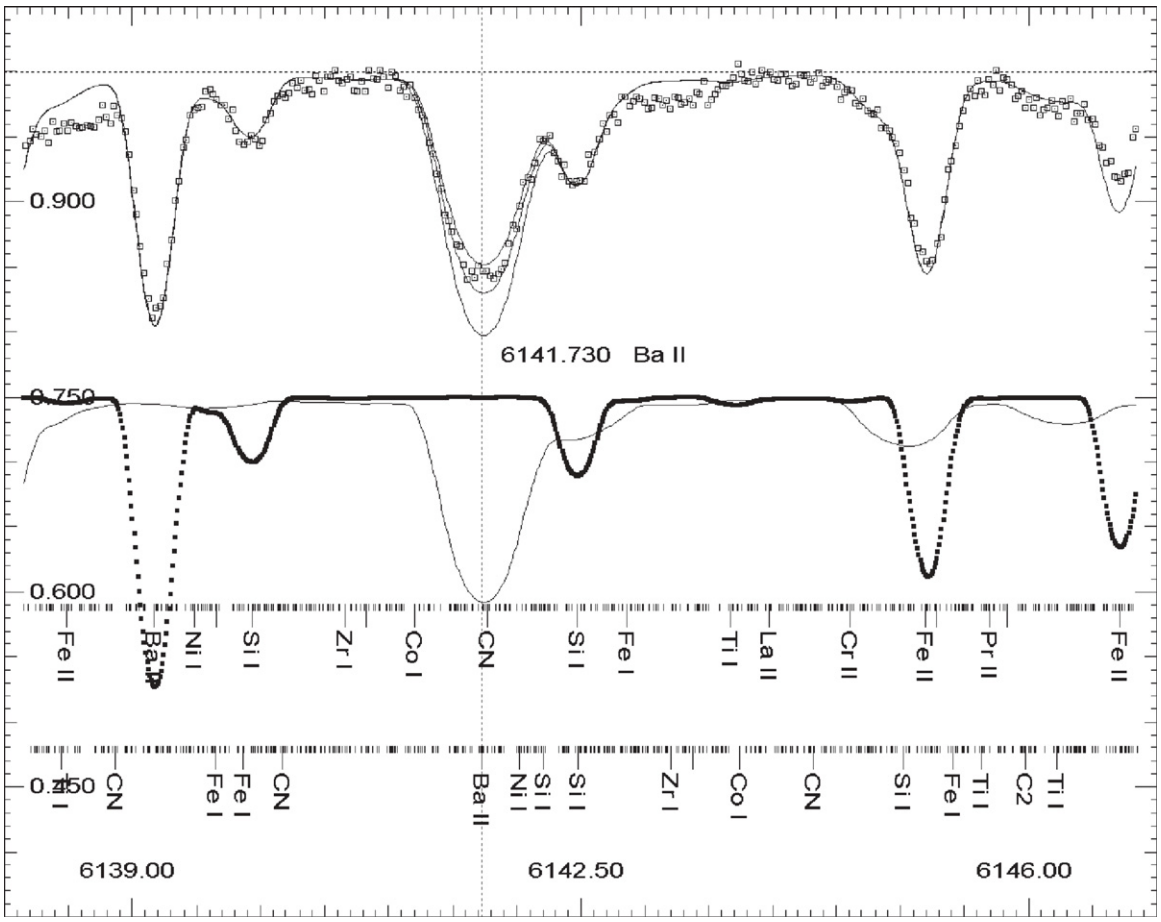

Figure 1. Spectrum of LX Per in the vicinity of the Ba II line λ6141.73. The axes are the wavelength in angstroms and the relative flux. In the top part of the figure, open squares are the observed spectrum. The solid line is the sum of the synthetic spectra of the components. Three synthetic spectra are shown near the Ba line of the cooler component. These spectra were calculated with the best barium abundance, which deviated by ±0.5 dex from the best value. Scaled and shifted synthetic spectra of both components are shown separately in the middle part of the figure. Filled squares: hotter component; solid line: cooler component; calculations were made with the best barium abundances. The synthetic spectra of components are shifted in accordance with the observed radial velocities and smoothed by the instrumental and rotational profiles. The positions of spectral lines, which were taken into account in calculations, are marked by short and long dashes (faint and strong lines). Some strong lines are identified.

Iron abundances were calculated from individual lines for each point across a four-dimensional grid of parameters involving $T_{\rm eff}$, $\log g$, $v_{\rm micro}$, and L_A/L_B. For each point of this four-dimensional space, the coefficients of correlations between the equivalent widths, excitation potentials, wavelengths, and iron abundances were calculated as well as the scatter of the individual abundances. The correct atmospheric parameters were selected as those providing zero or close to zero correlation coefficients and minimal scatter in the derived iron abundances. The Kurucz (1993) grid of atmosphere models was used to interpolate sub-grids of models.

After several iterations, we found the following set of parameters for the hotter (A) and cooler (B) components: $T_{{\rm eff}\,A} = 6225 \pm 50$ K, $\log g_A = 3.92 \pm 0.05$, $\log N({\rm Fe})_A = 7.45 \pm 0.05$, and $v_{{\rm micro}\,A} = 2.0 \pm 0.05\,{\rm km\,s^{-1}}$ for the hotter component, and $T_{{\rm eff}\,B} = 5225 \pm 50$ K, $\log g_B = 3.42 \pm 0.05$, $\log N({\rm Fe})_B = 7.38 \pm 0.11$, and $v_{{\rm micro}\,B} = 3.4 \pm 0.05\,{\rm km\,s^{-1}}$ for the cooler component. The ratio of luminosities is $L_A/L_B = 0.90 \pm 0.05$ at the wavelength of 5550 Å. Figure 2 shows the correlations of iron abundances calculated for 72 iron lines of the cooler component versus the equivalent widths ($\log(W/\lambda)$), energies of low levels, and wavelengths of these lines.

The above-mentioned errors of derived parameters are the formal errors of the chosen method. Systematic errors are also possible. To estimate the level of possible systematic errors, we repeat these calculations with another grid of atmosphere models from Castelli & Kurucz (2003). The results for the cool component are shown in Figure 3. The temperature and the surface gravity of this component seem to be close to the above-mentioned values, but, as it will be shown in the next section, the temperature derived for the cooler component from the solution of light and radial velocity curves is significantly lower. The possible reasons for this discrepancy will be discussed in Section 5.

3.2. Projected Rotational Velocities

The projected rotational velocities ($v \sin i$) of the components were found using the Fourier transform of the observed spectrum. Clean lines of Fe and a few lines of O, Ti, and Ni longward of 5300 Å were used. The first roots of the Fourier transform were found for 12 and 11 lines in the spectra of the hot and cool components, respectively, and were compared with the Fourier transform of the synthetic spectrum and convolved with instrumental and rotational profiles for different values of the projected rotational velocities. The values of the projected rotational velocities of the hot and cool components were $v \sin i_A = 9.6 \pm 0.6\,{\rm km\,s^{-1}}$ and $v \sin i_B = 20.9 \pm 0.8\,{\rm km\,s^{-1}}$, respectively. Since LX Per is an eclipsing binary (with $i = 87.^{\circ}2$),

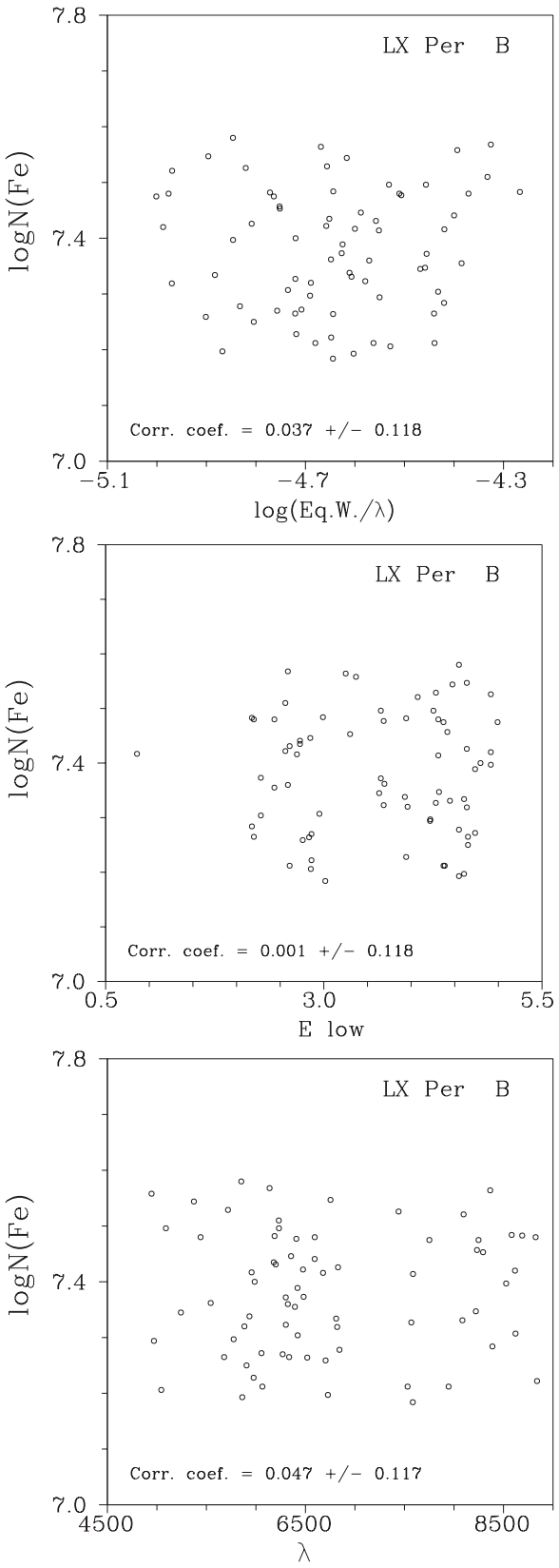

Figure 2. Correlation between the iron abundances in the atmosphere of the cooler component of LX Per determined from 72 lines of neutral iron and the equivalent widths (log(Eq.W./λ)), the excitation energies ($E_{\rm low}$), and the wavelengths (λ) of these lines. The correlation coefficients are indicated in the bottom parts of the panels. In accordance with Table 6, the error of each abundance value obtained from a single line of neutral iron is equal to ±0.11 dex.

these measured values are essentially the stars' rotational velocities. It should be pointed out that rotation was discussed as the unique broadening mechanism. Taking into account the macroturbulence can reduce the rotational velocities.

Using the same spectrum but a different method, Glazunova et al. (2008) found similar values of the projected rotational velocities of the components: $v \sin i_A = 9.1 \pm 0.6$ km s^{-1} and $v \sin i_B = 21.1 \pm 0.8$ km s^{-1}.

As will be shown, hereafter the radii of the components are 1.64 and 3.10 solar radius. These values and the orbital period of the system allowed us to find synchronized rotational velocities of the components equal to 10.3 and 19.5 km s^{-1} for the hotter and cooler components, respectively. These velocities are close to the observed values, so the rotation of the components seems to be nearly synchronized with the orbital period.

3.3. Calcium Emission Lines and Radial Velocities

Radial velocities of the components were estimated using 61 and 72 clean lines of neutral iron in the spectra of hotter and cooler components, respectively. Observed barycentric values of the radial velocities of the components $v_{rA} = -35.7 \pm 0.8$ km s^{-1} and $v_{rB} = +89.3 \pm 1.4$ km s^{-1} are in good agreement with those predicted with ephemerides calculated using Popper (1988) and our orbital elements, as illustrated in Figure 4.

LX Per is a chromospherically active RS CVn-type system that shows dominant Ca II H&K emission lines. It consists of F8–G0 V and G9–K0 IV components (Weiler 1974; Popper 1988).

We confirmed the strong Ca II H&K emissions and also found the emission line in the Ca II reversals' triplet absorptions at the wavelengths of 8498, 8542, and 8662 Å in the spectrum of LX Per. Therefore, five emission lines are plotted in Figure 5.

The emission lines were examined to determine which component of the system contributes to them. First, we measured the radial velocity of emission lines assuming that the emission lines dominated the center of the corresponding absorption lines. The radial velocities were $v_r = 89.3$, 89.0, 88.9, 89.9, and 90.3 km s^{-1} for Ca II H, Ca II K, Ca II λ8498, Ca II λ8542, and Ca II λ8662 lines, respectively. These values showed good agreement with the radial velocity of the cooler star of the system, which was pointed out earlier in this paper. The coincidence of the visible chromospheric emission features with the wavelengths of absorption lines of the cooler component showed definitively that this star exhibited chromospheric activity.

4. UNIQUE PHOTOMETRIC SOLUTION FOR EPOCHAL LIGHT CURVES WITH DIFFERENT MORPHOLOGIES

The photometric observations of LX Per have been reported by several investigators. The light curve analysis has been carried out by Popper & Dumont (1977) and Túmer et al. (1985). They found the shape of light curves to be asymmetric and continuously changing. However, Túmer et al. (1985) showed that light curve variations formed a wave-like distortion outside of the eclipse with an amplitude up to 0.08 mag. Popper & Dumont (1977) suggested that the outside eclipse light variations were due to tidal ellipticity and mutual irradiation.

In the previous section, we confirmed that LX Per shows strong emission line reversals of the Ca II H&K absorption lines as well as other strong Ca II absorption lines and they originate from the cooler more chromospherically active star. Close binaries with significantly deep convective envelopes were expected to have manifestations of magnetic activity such

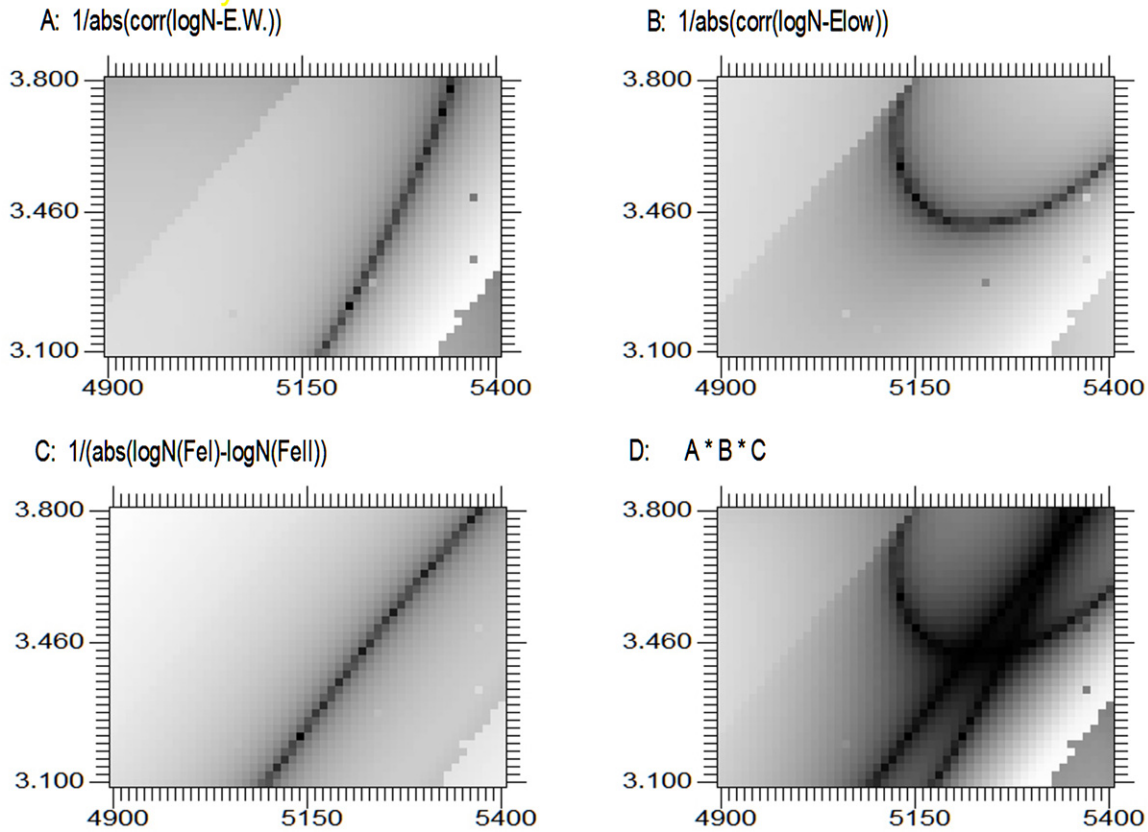

Figure 3. Determination of atmospheric parameters for the cooler component of LX Per with the Castelli & Kurucz (2003) grid of atmosphere models. The axes are the effective temperature and the surface gravity. The darkness of the points is proportional to the absolute reciprocal values of correlation coefficients for panels (A) and (B), and to the absolute reciprocal difference between the abundances of iron found using the lines of neutral and ionized species (panel C). Panel (D) is the multiplication of panels (A), (B), and (C).

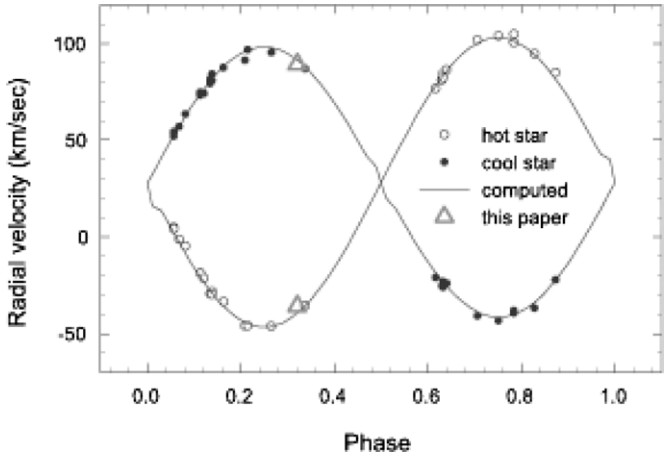

Figure 4. Radial velocity curves of LX Per.

as photospheric spots, chromospheric emission, and coronal X-ray and flare activity if the stars also had fast rotation. RS CVn binaries have especially low-amplitude quasi-sinusoidal light variations due to the presence of large dark starspots. The photometric wave appearing on a light curve migrates in the orbital phase.

Similar to other chromospherically active RS CVn stars, the emission lines of LX Per were explained as the chromospheric emission, and the wave-like distortion was due to dark spots on the cooler star of the system. Therefore, we selected and analyzed the distorted light curves of three epochs presented by Túmer et al. (1985) to find a unique solution, i.e., true orbital and geometric properties of LX Per.

Previous investigators presented different photometric solutions because the light curves they analyzed showed different light curve morphologies due to differing spot distributions. Thus, the unique photometric solution, which can explain various different shapes of light curves, was necessary for LX Per.

In order to find the unique photometric solution of LX Per, we first collected radial velocities from Weiler (1974) and Popper (1988). However, we analyzed only the radial velocities observed by Popper (1988) and those in this paper because those velocities show more accurate and better orbital phase coverage than those of Weiler (1974). We obtained a mass ratio of 1.07 ± 0.01, a semi-major axis of 23.1 ± 0.1 solar radii, and a system velocity of 28.24 ± 0.25 km s^{-1} by analyzing the double line radial velocity curves. Figure 4 shows the fitness of model radial velocity curves to the observed radial velocity curves.

Next, we analyzed the BV distorted light curves of three epochs presented by Ibanoglu et al. (1983) and Túmer et al. (1985). The radial velocity curves of LX Per are accurate enough to define the spectroscopic parameters. Thus, we fixed the spectroscopic parameters, such as mass ratio (q), system velocity (γ), and semi-major axis (a) of the orbit during the light curve analysis. We adopted the color index of LX Per binary system the $B - V = 0.88$ from the SIMBAD database. Taking into account the color index and the relation between effective temperature and $B - V$ presented by Surina (2008),

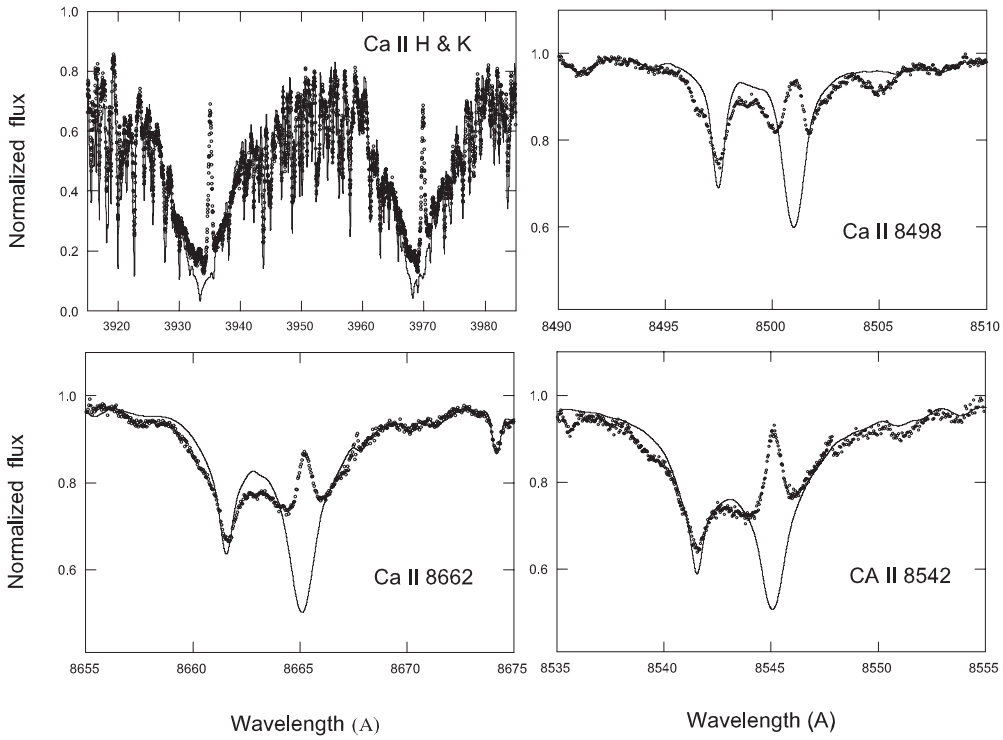

Figure 5. Plots showing the spectra centered on the Ca II H&K features as well as the Ca II triplet features at wavelengths of 8498, 8542, and 8662 Å. The observed and the synthetic spectra are shown by open squares and curved lines, respectively. The chromospheric emission reversal features arising from the K0 IV component are clearly seen.

we assumed the initial temperature of the primary star to be 6200 K. The initial linear limb-darkening coefficients (x_1, x_2) of the hotter and cooler stars were adopted from van Hamme (1993). The gravity-darkening exponents were assumed to be $g_1 = 1.00$ and $g_2 = 0.32$ based on their spectral types.

First, we produced the immaculate (unspotted) symmetrical model light curves, which were fit to the brighter maxima of the 1983 light curves which show good phase coverage for the eclipses as well as outside the eclipses. Mode 2 of the W-D code (i.e., the detached case) was used to adjust the orbital and geometric parameters of LX Per. As expected, the model light curves do not fit to the observed light curves, which are asymmetric, as mentioned earlier, due to the presence of starspots. Therefore, the starspot models were adopted to fit to the observed asymmetric light curves. A single large cool spot was employed for the cooler K0 IV star that contributes to enhancement of the Ca II emission lines. One spot has four parameters: stellar longitude, latitude, radius, and temperature factor (TF_s), which equals the local surface temperature divided by the local undisturbed surface temperature. A detailed description of spot model parameters can be found in Kang & Wilson (1989). The longitude, radius, and temperature factor of the spot have been adjusted to fit the observed light curve.

An additional unresolved problem is the latitude of the spot. A spot near the poles versus one near the equator would certainly make a measurable difference in the light curves. In the case of an eclipsing binary, a spot near a pole causes minimal disturbance with phase, and this disturbance should increase as the distance between the spot and the pole increases. The location of a spot near the equator evidently has the maximum influence on light curves. In this paper, we fixed the spot co-latitude at 80° (spot located 10° from the star's equator). We intend to consider the spot latitude as the adjustable parameter in future investigations.

The 1983 *B* and *V* light curves were asymmetric and appeared to have an unusual concave appearance near phase 0.75. The theoretical *B* and *V* light curves produced by the one spot model were successfully fitted to most observations. The spot is located at a longitude of 228.°4, making it most visible to the observer near phase 0.7–0.9. The fitted model light curves are plotted in Figure 6. The filled circles are the observations. The solid curves are the computed light curves with the spot.

The models with cool spot distributions seen at phases 0.0 and 0.5 are shown in the three-dimensional representation displayed at the top of the figure. The detailed fitting of the light curves at the primary minimum, shown in the left box of Figure 6, indicates an occultation (total eclipse). Therefore, the hot F9/G0 V star is eclipsed and only the K0 sub-giant star is visible at phase 0.0 in the three-dimensional representation.

The 1982 and 1981 light curves covered portions of the light curves only outside of the eclipses, but these light curves showed the distortion wave clearly. Therefore, we used the same system parameters as in the 1983 light curves to produce model light curves for the 1982 and 1981 epochs. The model light curves were fitted to the 1982 and 1981 observations successfully by adjusting only spot parameters. The 1982 and 1981 fitted model light curves are plotted along with the three-dimensional spotted components of the binary system in Figures 7 and 8, respectively. During 1981 and 1982, the spots were located at longitudes of 59.°1 and 311.°3, respectively. Thus, the spot migrated approximately 95° between 1981 and 1982.

It is necessary to find the temperatures of both components using the temperature ratio and radius ratio determined by the light curve analysis. The Wilson and Devinney differential

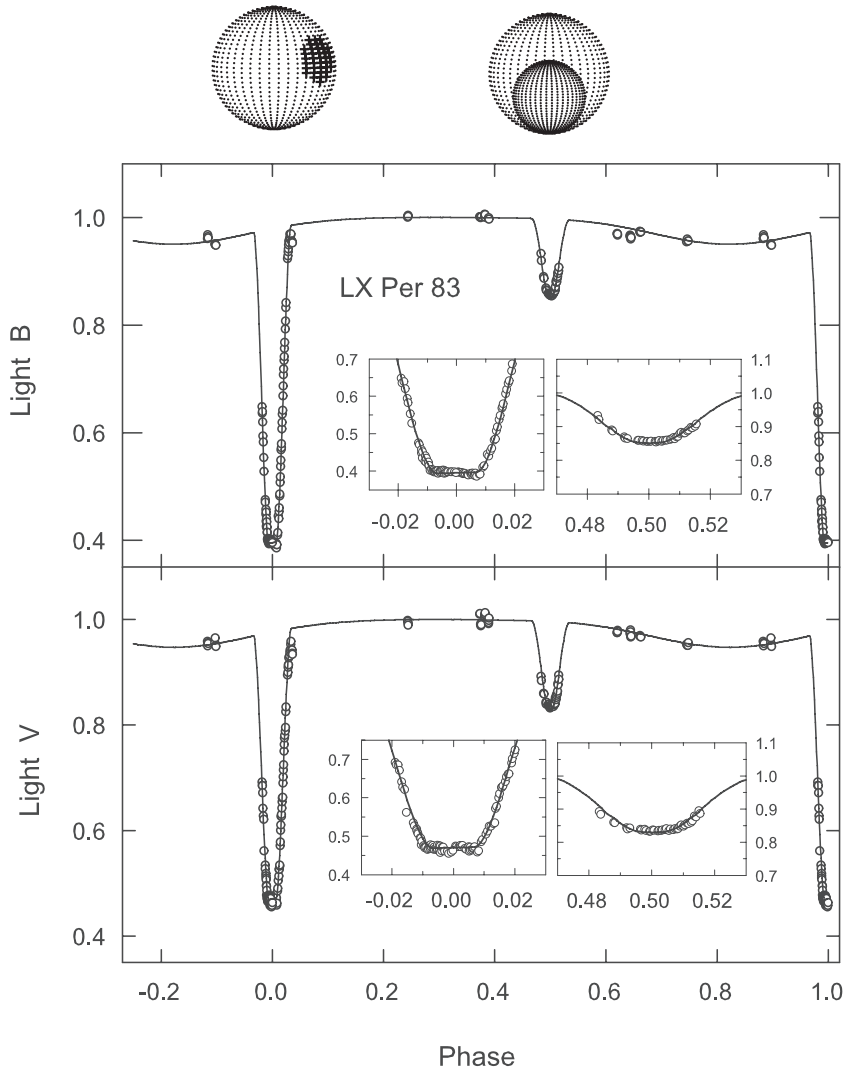

Figure 6. 1983 *B* and *V* light curves of LX Per are shown with the fitted model light curves. The open circles are the observations. The solid curves are the computed light curves with the spot. The figures in the boxes show detailed fitting at the primary and secondary minima. The primary eclipse shows a total occultation eclipse. The models with cool spot distribution seen at phases 0.0 and 0.5 are shown in the three-dimensional representation displayed at the top. The hotter G0V star is eclipsed and only the cooler K0 IV star is seen at phase 0.0.

correction program gives an accurate temperature ratio rather than the temperatures of the individual components because we use normalized light curves for the analysis. We found the temperature of each component of an eclipsing binary system using the method described by Kang et al. (2004). Accurate ratios of radii and temperatures for the binary system were necessary for this solution. Finally, we obtained temperatures of the primary star and the secondary star of the binary system as 6200 K and 4792 K, respectively.

Table 2 lists the orbital inclination (i), mass ratio (m_2/m_1), temperatures (T_1, T_2), potentials (Ω_1, Ω_2), albedos (A_1, A_2), gravity-darkening exponents (g_1, g_2), and limb-darkening coefficients (x_1, x_2) of both components, relative fluxes in B and V bandpasses and spot parameters such as the latitudes (θ), longitudes (λ), radii, and temperature effects (TF_s) of spots.

The calculated absolute properties of both stars are given in Table 3. We calculated the surface gravities $\log g$(cgs) as 4.10 and 3.58 for primary and secondary stars, respectively. Those values show agreement with surface gravities determined by the high dispersion spectrum in Section 3.1 within the error bars.

The distance of LX Per was calculated as 86.4 pc using the distance modulus based on an expected magnitude $m_V = 8.^{\rm m}1$ from Popper (1988); the absolute magnitude of the LX Per system was calculated as $M_V = 2.^{\rm m}8$, and the color excess $E_{B-V} = 0.^{\rm m}2$. This distance shows reasonably good agreement with the value of 100.0 ± 10.3 pc listed in the *Hipparcos* catalog (Perryman et al. 1997).

We estimated the spot effect (SE) defined by Kang (1993) as

$$\mathrm{SE} = (l' - l)/l, \quad (1)$$

where l is an observed flux at the phase of maximum SE so that this flux is reduced due to intrinsic variation including the spot. l' is the theoretical flux for an immaculate star at the same phase. The maximum SEs in the V light curve of LX Per are 0.052, 0.055, and 0.054 in the 1983, 1982, and 1981 epochs, respectively.

These values are typical for RS CVn-type binaries. Kang (1993) and Kang et al. (2002, 2003) found the SE to be 0.07–0.16 for SZ Psc, 0.02–0.04 for TY UMa, 0.11 for MM Her, and 0.08 for CF Tuc. These RS CVn-type binaries have light curves that are distorted by starspots on the surface of cooler stars. Table 4 lists the SE parameters for several binary stars.

The binary systemic parameters, including inclination, mass ratio, temperatures, and gravities of both components of

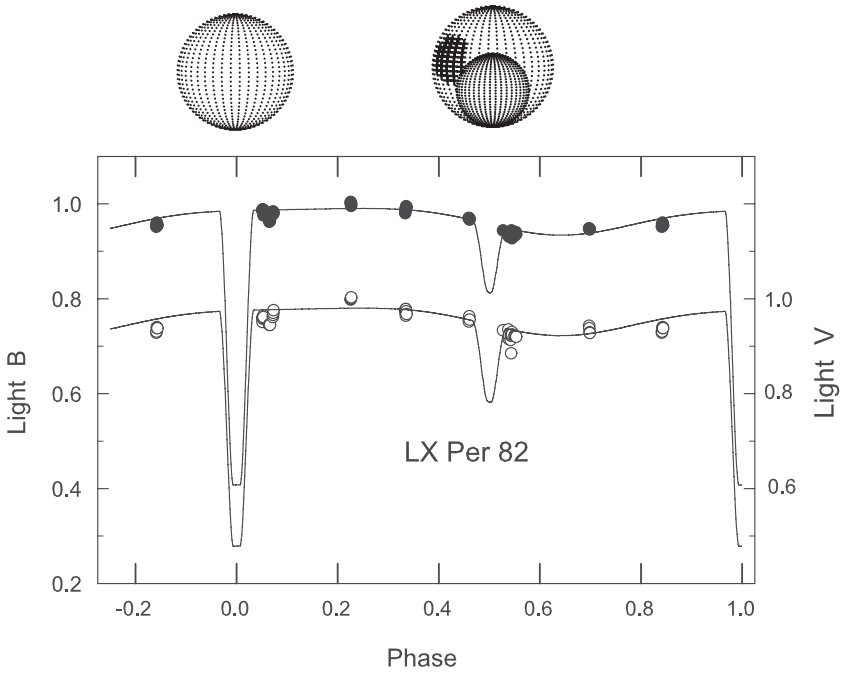

Figure 7. Same as Figure 6, but for 1982.

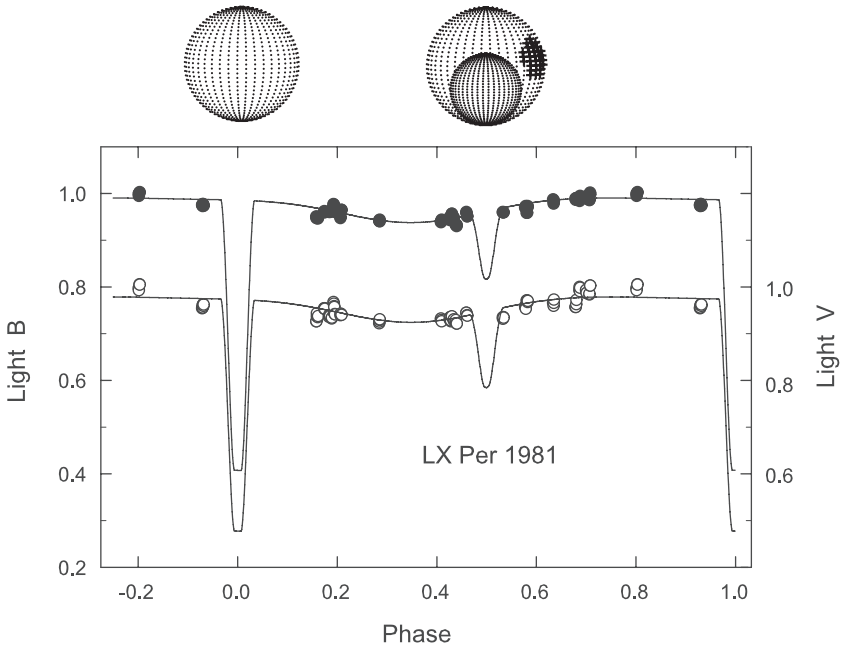

Figure 8. Same as Figure 6 but for 1981.

LX Per, for the three observations are nearly identical, although the shapes of light curves for three epochs are different from each other. Changing only the spot parameters, the model light curves fit the observed light curves for three epochs very well. This means that the variations of the spot location and size are the primary reasons for the observed variations in the shape of the light curves.

5. THE ADOPTED ORBITAL AND PHYSICAL PROPERTIES OF LX Per

Comparison of the temperatures of cool components of LX Per obtained from the light curve solution and from the spectral analysis of iron lines shows a significant difference. This apparent temperature difference cannot be explained by observational errors, which is why we tried to find the reason for this discrepancy. One of the possible reasons could be interstellar extinction. The star is located near the Galactic plane (galactic latitude $b = -8^{\circ}$), so we can expect interstellar medium reddening. Popper (1988) used $E_{B-V} = 0\overset{m}{.}04$, adopted from Perry & Johnston (1982) extinction maps.

We tried to estimate the extinction in the direction of LX Per using the data collected in the SIMBAD database. We analyzed A0 and B9 stars located in the circle with a radius of 4^{o} centered at LX Per. All stars in the central part of this circle show $B - V \geqslant 0.09$. The nearest stars are HD 19992 (spectrum A0) and HD 20022 (A0, parallax 8.47 mas). These

Table 2
Photometric Elements of LX Per

Parameters	1983	1982	1981
i	$87\overset{\circ}{.}51 \pm 0\overset{\circ}{.}03$	$87\overset{\circ}{.}51 \pm 0\overset{\circ}{.}06$	$87\overset{\circ}{.}51 \pm 0\overset{\circ}{.}06$
$q(m_2/m_1)$	1.067 ± 0.1	1.067 ± 0.1	1.067 ± 0.1
T_1	6200 K	6200 K	6200 K
T_2	4792 ± 32 K	4792 ± 32 K	4792 ± 32 K
Ω_1	15.13 ± 0.12	15.13 ± 0.12	15.13 ± 0.12
Ω_2	8.61 ± 0.02	8.61 ± 0.02	8.61 ± 0.02
A_1	0.5	0.5	0.5
A_2	0.5	0.5	0.5
g_1	1.00	1.00	1.00
g_2	0.32	0.32	0.32
x_{1B}	0.815	0.815	0.815
x_{2B}	0.855	0.855	0.855
x_{1V}	0.725	0.725	0.725
x_{2V}	0.808	0.808	0.808
$L_1/(L_1+L_2)_B$	0.583 ± 0.002	0.583 ± 0.002	0.583 ± 0.002
$L_1/(L_1+L_2)_V$	0.506 ± 0.002	0.506 ± 0.002	0.506 ± 0.002
Spot θ	$80\overset{\circ}{.}0$	$80\overset{\circ}{.}0$	$80\overset{\circ}{.}0$
Spot λ	$228\overset{\circ}{.}4 \pm 4\overset{\circ}{.}0$	$311\overset{\circ}{.}3 \pm 5\overset{\circ}{.}4$	$59\overset{\circ}{.}1 \pm 1\overset{\circ}{.}0$
Spot r_s	$21\overset{\circ}{.}7 \pm 0\overset{\circ}{.}4$	$22\overset{\circ}{.}8 \pm 0\overset{\circ}{.}4$	$19\overset{\circ}{.}4 \pm 0\overset{\circ}{.}3$
Spot TF	0.89 ± 0.04	0.86 ± 0.02	0.80 ± 0.03

Table 3
Absolute Properties of LX Per

Property	Hotter Star	Cooler Star
Mass	$1.24 \pm 0.03\ M_\odot$	$1.32 \pm 0.03\ M_\odot$
Radius (mean)	$1.64 \pm 0.06\ R_\odot$	$3.10 \pm 0.07\ R_\odot$
$T_{\rm eff}$	6200 ± 312 K	4792 ± 230 K
M_V	$3\overset{\rm m}{.}48 \pm 0\overset{\rm m}{.}34$	$3\overset{\rm m}{.}61 \pm 0\overset{\rm m}{.}21$
log g(cgs)	4.10 ± 0.13	3.58 ± 0.11
Luminosity	$3.52 \pm 0.31\ L_\odot$	$4.47 \pm 0.36\ L_\odot$
Distance (pc)	86.4	

stars are located at angular distances of $28'$ and $18'$ from LX Per and have $B-V$ values of $0\overset{\rm m}{.}25$ and $0\overset{\rm m}{.}22$, respectively. Note that the parallax of LX Per in accordance with *Hipparcos* data is 10.0 mas, so the distance to LX Per is less than the distance to HD 20022. We can conclude that interstellar reddening in the direction of LX Per can reach $E_{B-V} \sim 0\overset{\rm m}{.}2$.

In accordance with previous photometric investigations of LX Per (Popper & Dumont 1977; Túmer et al. 1985), the $B-V$ color of the cooler component is $0\overset{\rm m}{.}95$. The effective temperature of the cooler component found from our high-resolution spectrum is $T_{\rm eff} = 5225$ K. Using the $(B-V)$–$T_{\rm eff}$ calibration of Ramirez & Melendez (2005), we found an intrinsic value of $(B-V) = 0\overset{\rm m}{.}78$ for the star with the above $T_{\rm eff} = 5225$ K. Thus E_{B-V} is $+0\overset{\rm m}{.}17$ which is quite close to the above-mentioned value for the nearest stars.

Another reason for discrepancies could be the variability of the cooler component. As pointed out by Popper (1988), the amplitude of light variations of the system outside of eclipses is $0\overset{\rm m}{.}08$. The amplitude of light variations of the cooler component should be approximately twice this range since its light variation is diluted by the more luminous hotter component. This amplitude corresponds to the changes in the effective temperature of the cooler component by ~200 K.

In recent years, it was shown that the physical parameters of single stars and of similar stars in binary systems are distinct. Malkov (2003) showed that the radii and effective temperatures of unevolved main-sequence components of eclipsing binaries and those of single stars are systematically different.

Table 4
Spot Effect of RS CVn and W UMa Type Binaries

Star Name	Epoch	Spot Effect	References
MM Her	1967	0.111	Kang (1993)
CF Tuc	1967	0.077	Kang (1993)
TY UMa	1967	0.044	Kang et al. (2002)
SZ Psc	1981	0.168	Kang et al. (2003)
CE Leo	1989	0.055	Kang et al. (2004)
LX Per	1981	0.054	This paper
LX Per	1982	0.055	This paper
LX Per	1983	0.052	This paper

The difference between the radii of binary components and single stars can reach 0.2 in the logarithmic scale for spectral classes A and F. Ribas (2006) found that the radii of M dwarfs in binary systems are 5%–15% larger than the predicted values. The two above-mentioned investigations summarized the discrepancies discovered in different binary systems.

It should be noted that the gravitational influence of a binary companion in close binaries results in the higher densities and temperatures of stellar interiors in comparison with single stars (Sirotkin & Kim 2009), but the influence of this effect on the surface temperatures of LX Per components is small.

The discrepancy between the values of temperatures derived by different methods can be significantly higher than the formal errors of these methods as it was discussed, for example, by Kang et al. (2012) for another eclipsing binary system ZZ Boo. That is why it seems reasonable to accept that the uncertainties of a component's determined parameters can be as high as ±400 K for effective temperatures, ±0.2 dex for surface gravities, ±0.2 km s^{-1} for microturbulent velocities, and ±0.1 dex for iron abundances.

For example, Túmer et al. (1985) found the radius of the cooler component to be equal to 3.16 $R_\odot$; this is close to our determination but about 0.4 $R_\odot$ greater than that given by Popper & Ulrich (1977). Later, Popper (1999) used a higher value of the radius of the cooler component, $3.05 \pm 0.05\ R_\odot$. The difference in radii and temperatures (near 400 K) is definitely outside of the error boxes, so it is desirable to find or to discuss the reason for this discrepancy.

LX Per was one of the 14 *Hipparcos* eclipsing binaries used by Popper (1999) to define a radiative flux relation. Pribulla et al. (2000) pointed out that the radiative flux of LX Per as well as RT And, SZ Psc, and UV Psc is markedly below the value expected from the intrinsic $B-V$ index and *Hipparcos* distance relation derived by Popper (1999). This flux anomaly was ascribed to surface irregularities and spots blocking part of the outgoing flux in the visual spectral region. Pribulla et al. (2000) note that the visual magnitudes of these systems do not correspond to observed color indices or spectral types determined from the spectroscopy.

As was discussed above, the cooler component of LX Per shows strong calcium emission lines. In the following sections, we will describe the signs of accretion in the outer zones of both components. The result of this accretion is the X-ray flux of the LX Per system. X-ray emission was also found for RT And, SZ Psc, and UV Psc (Kashyar & Drake 1999).

All methods used in this paper were developed and calibrated for the stars with normal photospheres, or at least for the stars without significant anomalies. Is it possible to consider LX Per a system of normal stars? It seems surprising that different methods of deriving the effective temperatures of components

being used for photospheres under strong accretion result in values that differ only by 400 K. For example, Lee et al. (2005) derived the effective temperature of α Per and noted that the different investigators published the effective temperatures of this star in a range of 5967 K to 6750 K.

It is necessary to point out that our high-resolution spectrum and the photometry employed in the analysis were secured at different years, and for this reason we cannot exclude real-time variability of the cooler component. For the determinations of the chemical composition of the components, we adopted the effective temperatures and other parameters found from our high-resolution spectrum.

6. THE CHEMICAL ABUNDANCE OF COMPONENTS

All chemical abundance determinations, except for the neutral iron lines, were made using the spectrum synthesis method.

A synthetic spectrum of LX Per for the whole wavelength range facilitated the identification of spectral lines. Atomic and molecular lines from Kurucz (1993) as well as lines from Morton (2000), Biémont et al. (2002), Fuhr & Wiese (2006), and Piskunov et al. (1995) (partially from the VALD database), and other sources are included.

Isotopic splitting and hyperfine structure of the lines were taken into account for Li, Sc, V, Mn, Co, Cu, and Ba. The data for Ba lines were taken from François (1996), and for other elements from Kurucz (1995a). It should be noted that for all lines we tried to use counterparts in the solar spectrum, such that the differential abundances are not strongly influenced by splitting effects. For this purpose, the Delbouille et al. (1973) Liége atlas of the solar spectrum was used.

The spectrum synthesis method needs information about line broadening parameters. In our case, we took into account only the projected rotational velocities.

A list of the determined abundances for elements determined from the individual lines is presented in Table 1 (iron lines) and Tables 5 and 6 (other elements, hotter and cooler components).

The first five columns of Tables 5 and 6 contain the identification of line, the wavelength, the oscillator strength used, the reference to this value, and the excitation potential. The list of references is presented at the end of Table 6.

The next two columns show the abundances in the atmospheres of one of the components of LX Per and of the Sun.

The eighth column of the tables indicates the abundance of investigated elements in the atmosphere of one of the components of LX Per with respect to the corresponding solar value (Column 7). Grevesse et al. (2010) solar system abundances were used for lines without counterparts in the solar spectrum.

The next two columns are the levels of blending for the lines in the synthetic spectra of the corresponding component of LX Per and of the Sun (1.0 for a clean line, 0.0 for a strongly blended line).

Columns 11 and 12 show the depths of the lines in the synthetic spectra of the hot or cool component of LX Per and of the Sun. The levels of blending as well as the depths of the lines were calculated using synthetic spectra, which were unsmoothed with rotational and instrumental profiles.

The last two columns of the tables are the corrections to the abundances, listed in Column 6 for two different atmosphere models, with slightly altered atmospheric parameters, namely, for a gravity increased by 0.2 dex and for an effective temperature increased by 100 K, respectively. These values can be used to estimate the errors in abundance determinations due to improper selection of atmospheric parameters and also due to the fitting procedure.

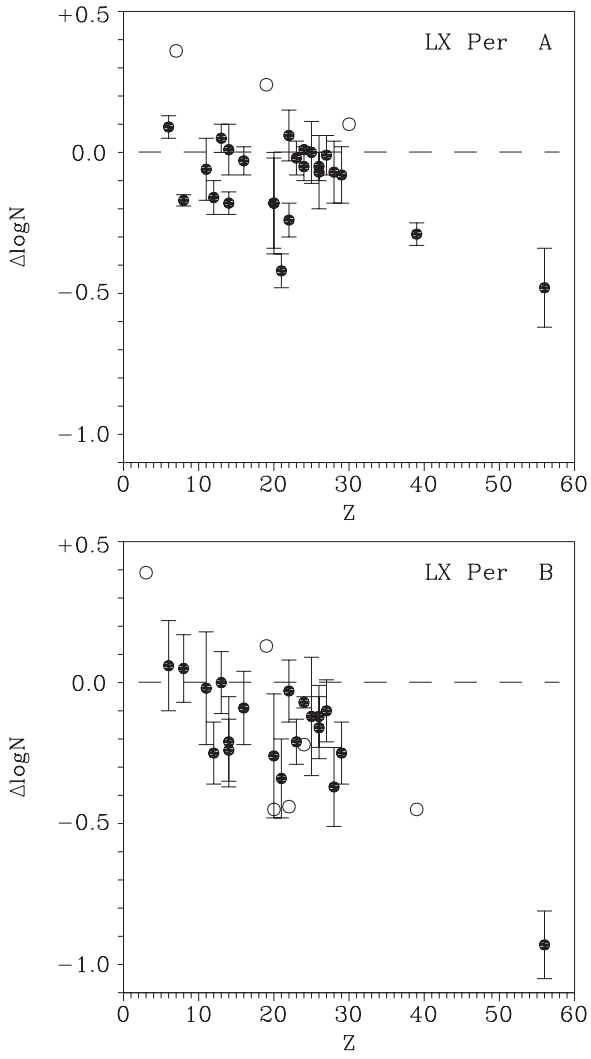

Figure 9. Chemical composition of the components of the LX Per system with respect to the Sun. The axes are the atomic numbers and the relative abundances. The open circles are the abundances of species determined from only one spectral line.

In Table 7, the mean elemental abundances in the atmospheres of the hotter and cooler components of LX Per are given. Both relative and absolute abundances of the chemical elements are shown. The first two columns are the atomic numbers and the identifications of the investigated species. The next column shows the numbers of spectral lines used. Two subsequent triplets of columns are the mean abundances in the atmosphere of LX Per for three sets of atmospheric parameters: the best values, the surface gravity shifted by +0.2 dex, and the effective temperature altered by +100 K. The absolute values for abundances are in the last three columns and the relative abundances are in the previous triplet. The final errors are shown in parentheses.

The abundances of 22 and 21 chemical elements were measured in the atmospheres of the hotter and cooler components, respectively. The results of our abundance determinations are illustrated in Figure 9. One of the barium lines is shown in Figure 1.

Table 5
Lines of Chemical Elements (Except Iron) in the Spectrum of the Hotter Component of LX Per

Ident.	λ	log gf	Ref.	E_{low}	log N		Δlog N	Blending		Depth in Synt.		Error for	
	(Å)			(eV)	(log N(H) = 12)		$*-\odot$	(1 = clean line)		Spectra		log g	T_{eff}
					LX Per	Sun		LX Per	Sun	LX Per	Sun	+0.2	+100 K
C I	4775.897	−2.304	r07	7.488	8.902	8.803	0.099	0.998	0.985	0.259	0.171	−0.023	0.073
C I	5380.337	−1.616	r07	7.685	8.449	8.397	0.052	0.993	0.981	0.244	0.174	−0.059	0.084
C I	6587.610	−1.330	r03	8.537	8.728	8.653	0.075	0.986	0.944	0.155	0.096	−0.068	0.059
C I	7111.472	−1.085	r07	8.640	8.376	8.304	0.072	0.974	0.965	0.110	0.068	−0.067	0.027
C I	7116.991	−0.910	r07	8.647	8.501	8.438	0.063	0.999	0.991	0.169	0.112	−0.049	0.059
C I	7860.882	−1.300	r08	8.851	8.665	8.499	0.166	0.996	0.987	0.085	0.042	−0.017	0.086
N I	8629.235	0.077	r02	10.690	8.252	7.891	0.361	0.936	0.569	0.067	0.025	−0.093	0.066
	...	...	...										

(This table is available in its entirety in machine-readable and Virtual Observatory (VO) forms in the online journal. A portion is shown here for guidance regarding its form and content.)

Table 6
Lines of Chemical Elements (Except Iron) in the Spectrum of the Cooler Component of LX Per

Ident.	λ	log gf	Ref.	E_{low}	log N		Δlog N	Blending		Depth in Synt.		Error for	
	(Å)			(eV)	(log N(H) = 12)		$*-\odot$	(1 = clean line)		Spectra		log g	T_{eff}
					LX Per	Sun		LX Per	Sun	LX Per	Sun	+0.2	+100 K
Li I	6707.768	−0.240h	r05	0.000	1.443		0.393	0.000		0.000		0.103	0.011
C I	4775.897	−2.160	r06	7.488	8.792	8.803	−0.011	0.991	0.985	0.148	0.171	0.025	−0.013
C I	7113.178	−0.773	r07	8.647	8.096	8.238	−0.142	0.974	0.716	0.279	0.102	−0.443	−1.204
C I	7115.172	−1.473	r07	8.643	9.038	8.960	0.078	0.925	0.904	0.190	0.106	0.043	0.008
C I	7860.882	−1.300	r08	8.851	8.806	8.499	0.307	0.988	0.987	0.134	0.042	0.112	0.065
O I	7774.166	0.223	r07	9.146	8.930	8.752	0.178	1.000	0.998	0.366	0.323	−0.181	0.079
O I	7775.388	0.002	r07	9.146	8.663	8.734	−0.071	1.000	0.999	0.322	0.275	−0.109	0.074
	...	...	...										

References. (r01) Kurucz 1992; (r02) Wiese & Fuhr 2007; (r03) Hirata & Horaguchi 1995; (r04) Kurucz 1995b; (r05) Smith et al. 1998; (r06) Kurucz & Peytremann 1975; (r07) Ralchenko et al. 2010; (r08) solar log gf, this paper; (r09) Kelleher & Podobedova 2008; (r10) Ivans et al. 2006; (r11) Kurucz 1993; (r13) Kurucz 1995a; (r14) Biémont et al. 2011; (r15) François 1996.

(This table is available in its entirety in machine-readable and Virtual Observatory (VO) forms in the online journal. A portion is shown here for guidance regarding its form and content.)

7. SIGNS OF ACCRETION IN THE ABUNDANCE PATTERNS

The main feature of the chemical composition of both components is the apparent deficiency of heavy ($Z > 30$) elements. Only elements with strong lines, namely Y and Ba, were detected. The chemical composition of the hotter component is similar to the usual metallic line star abundance pattern, but without overabundances of $Z > 30$ elements.

To explain the abundance patterns of the components, it is worth noting that LX Per is an RS CVn-type binary. Systems of this type exhibit infrared excesses and chromospheric activity; gaseous and dust streams can also exist in these systems.

That is why we tried to plot the relative abundances of chemical elements in the atmospheres of components against the condensation temperatures and second ionization potentials (SIPs) of these elements. The results are shown in Figures 10 and 11.

The anticorrelation of relative abundances and condensation temperatures is observed in stars with dust envelopes (Venn & Lambert 1990, 2008). Both components of LX Per show the decrease of relative abundances with condensation temperatures. The correlation coefficients are equal to -0.51 ± 0.16 and -0.44 ± 0.18 for the hotter and cooler components, respectively. These enable us to consider the dust–gas separation mechanism as one of the phenomena responsible for the anomalous chemical composition of both components.

It is necessary to note that for stars with mainly radiative energy transport in their outer zones, such as λ Boo-type stars, this scenario can work at lower densities of gas and dust in the environment of the star because the stable atmospheres of these stars conserve the abundance anomalies, and atomic diffusion is able to destroy it only at timescales of a few millions of years. One can suppose that to make these anomalies detectable in the stars with mainly convective energy transport in their outer layers higher densities of gas and dust are required.

Chromospheric activity of the cooler component is clearly signed by calcium emissions. It should produce the strong stellar wind from this component and form the gaseous envelope of the system. Part of the atoms can be accreted back by both components, and it is natural to discuss the possibility of observational detection.

Due to the existence of a gaseous envelope around the binary system, the accretion can be continuous, and its intensity can exceed that of single stars. That is why it is possible to expect that the signs of accretion, which are usually observed in stars with mainly radiative energy transport in their outer layers, can also be detected in RS CVn-type stars.

As was mentioned above, the accretion of interstellar gas was proposed by Greenstein (1949) to explain the deficiency of

Table 7
Mean Abundances of Chemical Elements in the Atmosphere of LX Per

Z	Ident.	n	$\Delta \log N_{\mathrm{LX\ Per}-\odot}$			$\log N_{\mathrm{LX\ Per}}$		
			$*-\odot$	$\log g$+0.2	T_{eff}+100	$*$	$\log g$+0.2	T_{eff}+100
				Hotter component				
6	C I	6	0.09(04)	0.04(06)	0.15(05)	8.60(18)	8.55(18)	8.66(19)
7	N I	1	0.36	0.27	0.43	8.25	8.16	8.32
8	O I	2	−0.17(02)	−0.23(02)	−0.10(01)	8.61(04)	8.55(04)	8.68(04)
11	Na I	4	−0.06(11)	−0.03(08)	−0.06(11)	6.32(11)	6.35(07)	6.32(11)
12	Mg I	5	−0.16(06)	−0.10(05)	−0.16(11)	7.31(29)	7.37(28)	7.32(31)
13	Al I	2	0.05(05)	0.09(05)	0.04(04)	6.45(10)	6.49(10)	6.44(09)
14	Si I	21	0.01(09)	0.05(10)	0.01(10)	7.50(20)	7.54(19)	7.50(19)
	Si II	2	−0.18(04)	−0.25(03)	−0.08(07)	7.25(08)	7.17(07)	7.34(10)
16	S I	5	−0.03(05)	−0.10(09)	0.03(05)	7.10(05)	7.04(09)	7.16(04)
19	K I	1	0.24	0.31	0.27	5.27	5.34	5.30
20	Ca I	11	−0.18(16)	−0.10(16)	−0.18(16)	6.19(22)	6.27(23)	6.19(23)
	Ca II	2	−0.18(18)	−0.23(20)	−0.11(18)	6.16(18)	6.11(20)	6.23(18)
21	Sc II	3	−0.42(06)	−0.35(10)	−0.30(09)	2.69(20)	2.76(28)	2.81(26)
22	Ti I	4	0.06(09)	0.15(10)	0.05(09)	4.99(11)	5.08(11)	4.98(10)
	Ti II	2	−0.24(06)	−0.23(04)	−0.16(05)	4.66(11)	4.67(09)	4.74(10)
23	V I	2	−0.02(06)	0.07(03)	−0.02(08)	3.86(11)	3.95(08)	3.86(13)
24	Cr I	2	−0.05(05)	0.05(06)	−0.04(06)	5.59(05)	5.69(06)	5.60(06)
	Cr II	2	0.01(01)	−0.08(04)	0.02(06)	5.65(01)	5.56(04)	5.66(06)
25	Mn I	4	0.00(11)	0.11(07)	0.00(11)	5.32(16)	5.43(12)	5.32(16)
26	Fe I	52	−0.05(05)	0.03(05)	−0.06(05)	7.45(05)	7.53(05)	7.44(05)
	Fe II	8	−0.07(13)	−0.07(12)	0.01(13)	7.43(13)	7.43(12)	7.51(13)
27	Co I	4	−0.01(07)	0.04(03)	−0.01(08)	4.90(10)	4.95(13)	4.90(11)
28	Ni I	17	−0.07(11)	0.01(11)	−0.07(11)	6.16(16)	6.24(16)	6.16(16)
29	Cu I	2	−0.08(10)	0.02(09)	−0.08(09)	4.09(12)	4.18(11)	4.08(12)
30	Zn I	1	0.10	0.10	0.05	4.66	4.66	4.61
39	Y II	2	−0.29(04)	−0.31(02)	−0.22(02)	1.85(02)	1.83(09)	1.92(04)
56	Ba II	3	−0.48(14)	−0.40(14)	−0.44(12)	1.76(11)	1.84(10)	1.80(10)
				Cooler component				
3	Li I	1	0.39	0.50	0.40	1.44	1.55	1.45
6	C I	4	0.06(16)	−0.01(36)	−0.23(66)	8.68(35)	8.72(39)	8.71(33)
8	O I	2	0.05(12)	−0.09(09)	0.13(13)	8.80(13)	8.65(10)	8.87(14)
11	Na I	4	−0.02(20)	0.05(20)	−0.03(17)	6.31(07)	6.39(06)	6.30(08)
12	Mg I	7	−0.25(11)	−0.08(21)	−0.23(14)	7.29(13)	7.46(24)	7.30(16)
13	Al I	3	0.00(11)	0.09(10)	0.00(13)	6.40(11)	6.48(10)	6.39(14)
14	Si I	17	−0.21(16)	−0.19(17)	−0.16(15)	7.25(19)	7.28(18)	7.30(19)
	Si II	2	−0.24(11)	−0.27(11)	−0.20(15)	7.18(08)	7.15(07)	7.22(11)
16	S I	3	−0.09(13)	−0.10(17)	−0.10(16)	7.04(15)	7.03(18)	7.04(17)
19	K I	1	0.13	0.29	0.12	5.16	5.32	5.15
20	Ca I	11	−0.26(22)	−0.14(21)	−0.27(20)	6.10(24)	6.21(23)	6.09(23)
	Ca II	1	−0.45	−0.48	−0.38	5.89	5.86	5.96
21	Sc II	6	−0.34(14)	−0.37(15)	−0.30(13)	2.74(20)	2.71(23)	2.79(20)
22	Ti I	6	−0.03(11)	0.09(12)	−0.01(12)	4.92(11)	5.04(12)	4.94(12)
	Ti II	1	−0.44	−0.54	−0.35	4.51	4.41	4.60
23	V I	4	−0.21(08)	−0.08(08)	−0.20(08)	3.70(09)	3.82(09)	3.70(09)
24	Cr I	4	−0.07(02)	0.03(02)	−0.08(01)	5.61(06)	5.71(07)	5.61(07)
	Cr II	1	−0.22	−0.31	−0.28	5.42	5.33	5.36
25	Mn I	7	−0.12(21)	−0.03(17)	−0.11(21)	5.29(27)	5.38(23)	5.30(27)
26	Fe I	72	−0.12(11)	−0.03(11)	−0.12(11)	7.38(11)	7.47(11)	7.38(11)
	Fe II	6	−0.16(11)	−0.20(11)	−0.06(11)	7.34(11)	7.30(11)	7.44(11)
27	Co I	7	−0.10(11)	−0.03(17)	−0.14(17)	4.81(11)	4.88(16)	4.77(14)
28	Ni I	24	−0.37(14)	−0.29(13)	−0.35(14)	5.87(18)	5.95(18)	5.89(19)
29	Cu I	4	−0.25(11)	−0.22(14)	−0.26(14)	3.89(09)	3.92(16)	3.88(11)
39	Y II	1	−0.45	−0.45	−0.36	1.63	1.63	1.72
56	Ba II	2	−0.93(12)	−0.86(10)	−0.87(15)	1.34(21)	1.41(19)	1.40(24)

chemical elements with SIPs close to the ionization potential of hydrogen (13.6 eV) in the atmospheres of metallic-line stars.

Later, Havnes (1971) proposed this type of accretion to explain the breaking of the rotation of magnetic stars and also as one of the sources of cosmic rays. North (1984) showed that this assumption was not confirmed by observations at that time. Böhm-Vitense (2006) considered charge-exchange reactions, which are the result of these accretion scenarios, as one of the reasons for the anomalous chemical composition of Am stars. All these investigators discussed

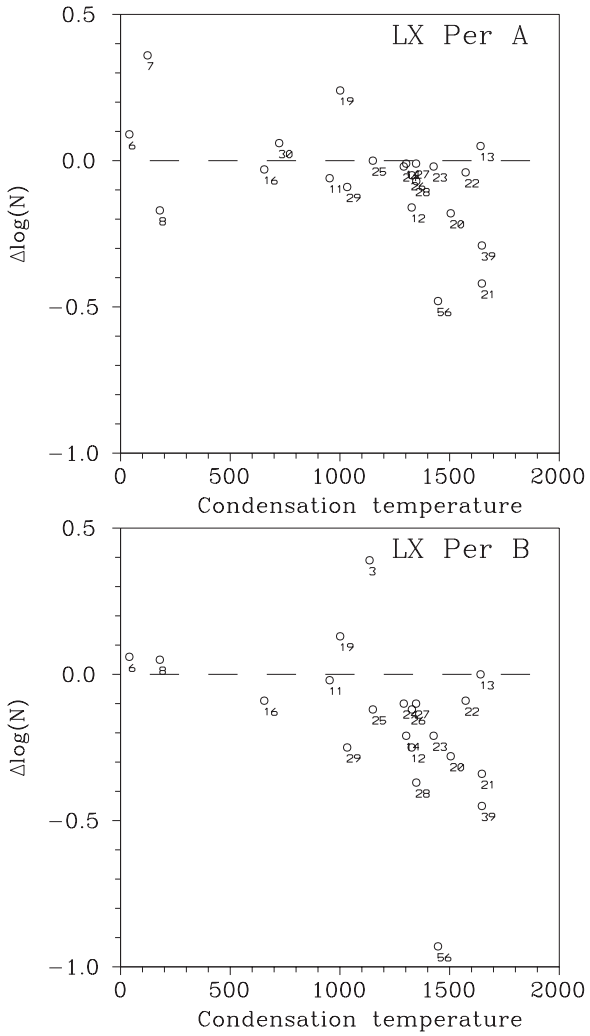

Figure 10. Plot of relative surface abundances of chemical elements in the atmospheres of components of LX Per as a function of the condensation temperatures of these elements. The values of condensation temperatures for a solar photosphere composition gas are taken from Lodders (2003). The atomic numbers of the elements are marked near the corresponding points. For elements observed in two ionization stages, the weighted mean values were adopted for this figure and the next one.

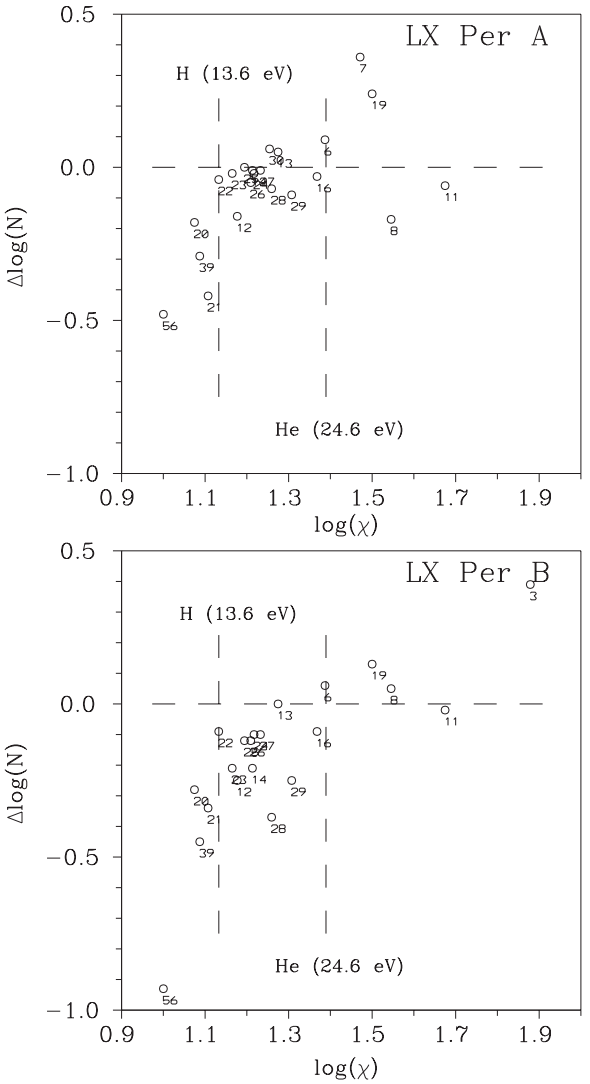

Figure 11. Plot of relative surface abundances of chemical elements in the atmospheres of components of LX Per vs. the SIPs of these elements. The atomic numbers of elements are marked. The vertical dotted lines are the ionization energies of hydrogen and helium (13.6 and 24.6 eV, respectively).

only single stars and the accretion of gas from an interstellar environment.

As it was pointed above, the components of LX Per have mainly convective energy transport in their outer zones but the density of gas in a binary system is expected to be much higher in comparison with a typical interstellar environment. As it is shown in Figure 11, the relative deficiency of elements with SIPs close to the ionization energy of hydrogen is observed in both components of LX Per.

The relative abundances of calcium, yttrium, and scandium in the atmosphere of the hotter component are lower than those of other elements except barium, but the condensation temperature of barium is higher, so this element should be strongly influenced by the dust–gas separation mechanism (Venn & Lambert 1990, 2008).

The relative abundance of titanium is higher than those of the above-mentioned three elements, but it should be noted that titanium shows higher values of relative abundances in most of the stars discussed by Böhm-Vitense (2006).

For the cooler component, a correlation of relative abundance with SIPs is clearly observed, and the correlation coefficient is 0.69 ± 0.11.

For both components, the relative abundances are clearly dependent on SIPs. The theory of charge-exchange reactions, which are responsible for these dependencies, is not developed for stellar atmospheres. We can only point to Havnes (1971), and his later papers. After North (1984), nobody tried to discuss this problem for two decades.

The relative underabundances of calcium can also be explained in the frame of diffusion theory. One example is *o* Leo (Michaud & Richer 2005). The main component of this binary system ($T_{\rm eff} = 6100$ K, $\log g = 3.25$) resembles the hotter component of LX Per, but its chemical composition is close to the abundance patterns of Am stars (Griffin 2002).

How can we explain the chemical composition of the components of LX Per? It seems reasonable to accept that two different accretion scenarios discussed above took place in this binary system. The interaction of these two types of accretion seems to be sufficient for understanding the main features of abundance patterns. Unfortunately, it is only a qualitative picture.

The quantitative model can be constructed after additional investigation of charge-exchange reactions and taking into account the possible effects of diffusion theory.

This investigation as well as the results of Kang et al. (2012) attract attention to accretion in binary systems as a physical phenomenon that can be important for understanding the observed properties of these systems. The possibility of accretion should not be neglected by future researchers.

8. CONCLUSIONS

We made echelle spectroscopic observations of LX Per and analyzed this spectrum and the archived B and V light curves. The findings from these analyses are summarized below:

1. By comparing the synthetic spectra of the binary system with the observed spectrum, we found the following parameters: $T_{\rm eff\,A} = 6225 \pm 350$ K, $\log g_A = 3.92 \pm 0.20$, $v_{\rm micro\,A} = 2.0 \pm 0.2\,{\rm km\,s^{-1}}$ for the hotter component and $T_{\rm eff\,B} = 5225 \pm 350$ K, $\log g_B = 3.42 \pm 0.20$, $v_{\rm micro\,B} = 3.4 \pm 0.2\,{\rm km\,s^{-1}}$ for the cooler component.
2. We confirmed the chromospheric activity of LX Per, detected its connection to the cooler component by comparing the radial velocities of emission lines with the radial velocity of this star, and found calcium emission lines in the infrared spectral region.
3. The unique solution could be obtained by adopting the starspot model for the light curves of three different epochs. Changing only spot parameters, the model light curves fit to the different shapes of observed light curves for three epochs. This means that the variation of the spot location and size is the main reason for the changing shape of the light curves. We also obtained the absolute properties and distance of LX Per.
4. The abundances of 22 and 21 chemical elements in the atmospheres of the hotter and cooler components, respectively, are found. The main chemical composition feature of both components is the apparent deficiency of heavy ($Z > 30$) elements. Only elements with strong lines, namely Y and Ba, were detected.
5. The relative abundances of chemical elements in the atmospheres of both components are clearly dependent on the condensation temperatures and on the SIPs of these elements. This can be explained by the accretion of dust and gas on the surface of the components.

We used the data from NASA ADS, SIMBAD, CADC, VALD, NIST, and DREAM databases, and we thank the teams and administrations of these programs and archives.

This research was supported in part by the General Researcher Program 2011-0010696 and Mid-career Researcher Program 2011-0028001, respectively, through the National Research Foundation (NRF) of Korea funded by the Ministry of Education.

REFERENCES

Biémont, E., Blagoev, K., Engstrom, K., et al. 2011, MNRAS, 414, 3350
Biémont, J., Palmeri, P., & Quinet, P. 2002, Database of Rare Earths at Mons University, http://www.umh.ac.be/~astro/dream.shtml
Böhm-Vitense, E. 2006, PASP, 118, 419
Castelli, F., & Kurucz, R. 2003, in IAU Symp. 210, Modelling of Stellar Atmospheres, ed. N. E. Piskunov, W. W. Weiss, & D. F. Gray (San Francisco, CA: ASP), Poster Contributions, A20, http://astrosociety.org/astroshop/index.php?p=product&id=133&parent=8
Caton, D. B. 1986, AJ, 91, 132
Chiavassa, A., Bigot, L., Kervella, P., et al. 2012, A&A, 540, 5
Cowley, C. 1977, Ap&SS, 51, 349
Delbouille, L., Roland, G., & Neven, L. 1973, Photometric Atlas of the Solar Spectrum from λ3000 to λ10000 (Liége: Institut d'Astrophysique de l'Universite' de Liege)
Drobyshevski, E. M. 1975, Ap&SS, 35, 403
Fowler, W. A., Burbidge, E. M., Burbidge, G. R., & Hoyle, F. 1965, ApJ, 142, 423
François, P. 1996, A&A, 313, 229
Fuhr, J. R., & Wiese, W. L. 2006, JPCRD, 35, 1669
Glazunova, L. V., Yushchenko, A. V., Tsymbal, V. V., et al. 2008, AJ, 136, 1736
Gopka, V. F., Yushchenko, A. V., Mishenina, T. V., et al. 2004, ARep, 48, 577
Goriely, S. 2007, A&A, 466, 619
Greenstein, J. L. 1949, ApJ, 109, 121
Grevesse, N., Asplund, M., Sauval, A. J., & Scott, P. 2010, Ap&SS, 328, 179
Griffin, R. E. 2002, AJ, 123, 988
Havnes, O. 1971, A&A, 13, 52
Hirata, R., & Horaguchi, T. 1995, SIMBAD Catalog VI/69, available at http://cdsarc.u-strasbg.fr/viz-bin/Cat
Ibanoglu, C., Evren, S., Túmer, O., Ertan, A. Y., & Tunca, Z. 1983, Ap&SS, 95, 409
Ivans, I. I., Simmerer, J., Sneden, C., et al. 2006, ApJ, 645, 613
Kang, Y. W. 1993, in ASP Conf. Ser. 38, New Frontiers in Binary Star Research, ed. K.-C. Leung & I.-S. Nha (San Francisco, CA: ASP), 371
Kang, Y. W. 2008, JASS, 25, 77
Kang, Y. W. 2010, JASS, 27, 75
Kang, Y. W., Lee, H.-W., Hong, K. S., Kim, C.-H., & Guinan, E. F. 2004, AJ, 128, 846
Kang, Y. W., Lee, W.-B., Kim, H.-I., & Oh, K.-D. 2003, MNRAS, 344, 1227
Kang, Y. W., Oh, K.-D., Kim, C. H., et al. 2002, MNRAS, 331, 707
Kang, Y. W., & Wilson, R. E. 1989, AJ, 97, 848
Kang, Y. W., Yushchenko, A., Hong, K., Kim, S., & Yushchenko, V. 2012, AJ, 144, 35
Kashyar, V., & Drake, J. J. 1999, ApJ, 524, 988
Kelleher, D. E., & Podobedova, L. I. 2008, JPCRD, 37, 267
Kim, K. M., Jang, J. G., Chun, M. Y., et al. 2000, PKAS, 15S, 119 (in Korean)
Kurucz, R. 1992, RMxAA, 23, 45
Kurucz, R. L. 1993, CD-ROMs No. 1–18 (Cambridge, MA: Smithsonian Astrophysical Observatory)
Kurucz, R. L. 1995a, CD-ROM No. 23 (Cambridge, MA: Smithsonian Astrophysical Observatory)
Kurucz, R. L. 1995b, in ASP Conf. Ser. 81, Workshop on Laboratory and Astronomical High Resolution Spectra, ed. A. J. Sauval, R. Blomme, & N. Grevesse (San Francisco, CA: ASP), 583
Kurucz, R. L., & Peytremann, E. 1975, SAO Special Report V, 362, part 1 (Cambridge, MA: Smithsonian Institution)
Lee, B. C., Galazutdinov, G. A., Han, I., et al. 2005, PASP, 118, 636
Lodders, K. 2003, ApJ, 591, 1220
Malkov, O. 2003, A&A, 402, 1055
Michaud, G. 1970, ApJ, 160, 641
Michaud, G. 2004, in IAU Symp. 224, The A-Star Puzzle, ed. J. Zverko, J. Ziznovsky, S. J. Adelman, & W. W. Weiss (Cambridge: Cambridge Univ. Press), 173
Michaud, G., & Richer, J. 2005, ApJ, 623, 442
Morton, D. C. 2000, ApJS, 130, 403
North, P. 1984, A&A, 141, 328
Percy, J. R. 1985, JRASC, 79, 113
Percy, J. R., & Welch, D. L. 1982, JRASC, 76, 185
Perry, L. C., & Johnston, L. 1982, ApJS, 50, 451
Perryman, M. A. C., Lindegren, L., Kovalevsky, J., et al. 1997, A&A, 323, 49
Piskunov, N. E., Kupka, F., Ryabchikova, T. A., Weiss, W. W., & Jeffery, C. S. 1995, A&AS, 112, 525
Poe, C. H., & Eaton, J. A. 1985, ApJ, 289, 644
Popper, D. M. 1988, AJ, 96, 1040
Popper, D. M. 1999, PASP, 110, 919
Popper, D. M., & Dumont, P. J. 1977, AJ, 82, 216
Popper, D. M., & Ulrich, R. K. 1977, ApJL, 212, L131
Pribulla, T., Chochol, D., Milano, L., et al. 2000, A&A, 362, 169
Proffitt, C. R., & Michaud, G. 1989, ApJ, 345, 998
Ralchenko, Yu., Kramida, A. E., & Reader, J. NIST ASD Team. 2010, NIST Atomic Spectra Database (version 4.0), http://physics.nist.gov/asd
Ramirez, I., & Melendez, J. 2005, ApJ, 626, 465
Ribas, I. 2006, Ap&SS, 304, 89
Shulyak, D., Ryabchikova, T., Kildiyarova, R., & Kochukhov, O. 2010, A&A, 520, 88
Sirotkin, F. V., & Kim, W.-T. 2009, ApJ, 698, 715
Smith, V. W., Lambert, D. L., & Nissen, P. E. 1998, ApJ, 506, 405

Ströhmeier, W. 1962, IBVS, 9, 1
Surina, F. 2008, MS thesis, Sejong Univ.
Tody, D. 1986, Proc. SPIE, 627, 733
Túmer, O., Ibanoglu, C., Evren, S., & Tunca, Z. 1985, Ap&SS, 112, 273
Van Hamme, W. 1993, AJ, 106, 2096
Venn, K. A., & Lambert, D. L. 1990, ApJ, 363, 234
Venn, K. A., & Lambert, D. L. 2008, ApJ, 677, 572
Weiler, E. J. 1974, PASP, 86, 56
Weiler, E. J. 1978, MNRAS, 182, 77
Wiese, W. L., & Fuhr, J. R. 2007, JPCRD, 36, 1287
Yushchenko, A. V., Gopka, V. F., Khokhlova, V. L., Musaev, F. A., & Bikmaev, I. F. 1999, AstL, 25, 453
Yushchenko, A. V., Gopka, V. F., Khokhlova, V. L., et al. 2004, A&A, 425, 171